10 April 1964, Volume 144, Number 3615 **SCIENCE**

Molecular Beam Scattering at Thermal Energies

Observations of atomic and molecular collisions yield information on the neutral-particle interactions.

Richard B. Bernstein

The observation of the scattering of molecular beams by gases is as old as the original discovery of the "molecular ray" by Dunoyer (*1*) in 1911. In the 1920's a number of semiquantitative studies of scattering were carried out (*2*). These consisted of measurements of the mean free path for molecular beams passing through gases at low pressure. Effective collision cross sections calculated from such mean-free-path data were comparable to, but generally larger than, the so-called "kinetic theory cross sections" based on transport properties (for example, viscosity and diffusion). More accurate and extensive experiments of a similar nature followed (*3–5*) during the 1930's; it was then recognized that precise measurements of scattering would yield, in a direct way, valuable information on the laws of interaction between the colliding molecules on a microscopic scale, from which the macroscopic gas properties could be calculated with the aid of statistical mechanical procedures.

The concept of an effective molecular collision cross section, usually designated Q (or σ), has been a useful one. It is defined as $Q = \pi r_0^2$, such that the actual collision rate would be reproduced by a calculation of the collision rate assuming the molecules to be hard spheres of diameter r_0. In general, molecular-collision cross sections depend upon the incident relative velocity v_r; usually Q decreases with increasing v_r.

The cross section may be expressed in terms of the attenuation of a monoenergetic molecular beam passing through a "static" target gas of known density:

$$\frac{I}{I_0} = e^{-nlQ} = e^{-l/\lambda} \qquad (1)$$

where I/I_0 is the transmittance, l is the length of the scattering zone, n is the number density of target molecules, Q is the cross section (*6*), and $\lambda = 1/nQ$ is the mean free path of the beam molecules.

Usually, Maxwellian velocity distribution of beam and target gases are involved, so the cross sections or mean free paths obtained from measurements of I/I_0 by means of Eq. 1 are averages over the velocity distributions (*4, 7, 8*). The symbol Q_{eff} has been used (*8*) to designate the "effective" cross section; that is,

$$Q_{\mathrm{eff}} = \frac{1}{nl} \ln \frac{I_0}{I} \qquad (2)$$

The true cross section is related to Q_{eff} by a (dimensionless) factor which is a function of the temperatures of the beam source and scattering gas and the appropriate velocity distribution functions.

The angular distribution of the scattering is also of considerable interest. Simple considerations suggest that the low-angle scattering is sensitive primarily to the long-range attractive interaction, while the large-angle scattering yields information mainly about the short-range repulsive forces (*9*). The earliest measurements (*10–12*) indeed showed the expected strong forward peak in scattered intensity arising from the long-range intermolecular attractive forces.

The angular distribution is described in terms of the so-called "differential" scattering cross section, defined as follows (for the simple case of scattering by a spherically symmetrical potential).

Let $d\dot{n}_{12}$ be the number of collisions occurring per unit time per unit volume between molecules moving with relative speed v_r, for which the relative velocity vector $\mathbf{v}_r$ is rotated by an angle in the range between θ and $\theta + d\theta$. Then

$$d\dot{n}_{12} = n_1 n_2 v_r \frac{d\sigma(\theta)}{d\Omega} 2\pi \sin\theta \, d\theta \qquad (3)$$

where n_1 and n_2 are the particle densities of the beam and target molecules, respectively, and $d\sigma(\theta)/d\Omega$ [sometimes designated $I(\theta)$] is the differential solid-angle scattering cross section for the specified v_r. The latter is expressible in units of, say, square angstroms per steradian.

Integrating over all scattering angles θ, one obtains the total rate (per unit volume) of collisions characterized by a relative speed v_r:

$$\dot{n}_{12} = n_1 n_2 v_r \, \sigma(v_r) \qquad (4)$$

where

$$\sigma(v_r) = 2\pi \int_0^{\pi} \frac{d\sigma(\theta)}{d\Omega} \sin\theta \, d\theta$$

is the total cross section mentioned earlier.

Two problems arise in connection with the interpretation of measured angular distributions in terms of differential scattering cross sections. First, as in the case of total cross sections, the velocity distributions in the beam and scattering gas must be taken into account. Second, one must ascertain the relation between the scattered intensity

---

The author is professor of physical chemistry at the University of Wisconsin, Madison, and a member of the university's Theoretical Chemistry Institute.

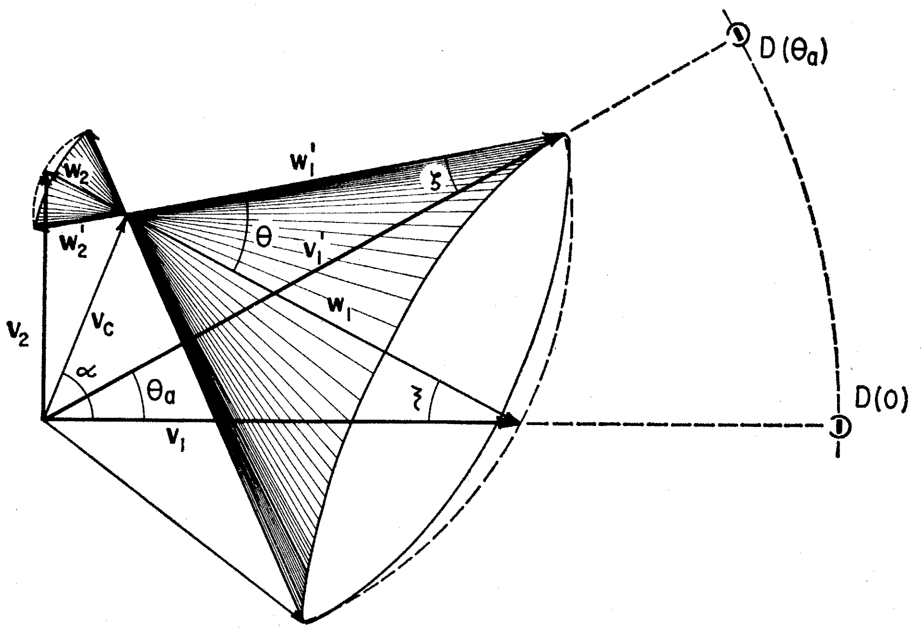

Fig. 1. Velocity diagram showing the relation between quantities in the apparatus and center-of-mass systems. Here $\mathbf{v}_1$ and $\mathbf{v}_2$ are the velocities of colliding particles 1 and 2; $\mathbf{v}_c$ is the centroid velocity; $\mathbf{w}_1$ is the velocity of particle 1 with respect to the center of mass; $\mathbf{v}_r$ (not explicitly shown) is the relative velocity (that is, $\mathbf{v}_r = \mathbf{v}_1 - \mathbf{v}_2 = \mathbf{w}_1 - \mathbf{w}_2$); $\mathbf{v}_1'$ is the velocity of particle 1 after collision; θ is the angle of deflection of the relative velocity vector due to the collision; and θ_a is the apparatus angle at which the detector is set, corresponding to the center-of-mass deflection angle θ.

as measured in the laboratory and that in the center-of-mass system. The latter problem is discussed briefly in the next section.

Conversion of Data to the Center-of-Mass System

In the limiting case of a heavy, essentially stationary "target" particle and a light, fast "beam" projectile, the laboratory and the center-of-mass systems are the same, so the differential cross section is directly proportional to the measured scattered current received by a detector subtending a constant solid angle at the scattering center, oriented at an angle θ from the beam axis.

In the general case, the angle of scattering in the laboratory or apparatus system, θ_a, differs from the angle, θ, in the center-of-mass system, and the differential cross section calculated from the observed scattered signal must be corrected by multiplication by the appropriate solid-angle ratio to obtain the true differential cross section in the center-of-mass system:

$$\frac{\mathrm{d}\sigma(\theta)}{\mathrm{d}\Omega} = \frac{\mathrm{d}\sigma(\theta_a)}{\mathrm{d}\Omega_a} \cdot \frac{\mathrm{d}\Omega_a}{\mathrm{d}\Omega} \qquad (6)$$

It is instructive to consider a simple case of practical interest in which two crossed beams intersect at right angles and the detector is confined to the plane of the beams. A "velocity diagram" for elastic scattering is shown in Fig. 1 (also see cover). We assume two collimated, monoenergetic beams of particles, of masses m_1 and m_2, with velocities $\mathbf{v}_1$ and $\mathbf{v}_2$ (in the present case $\mathbf{v}_1 > \mathbf{v}_2$). In Fig. 1, $\mathbf{v}_c$ designates the velocity of the center of mass; $\mathbf{v}_r = \mathbf{v}_1 - \mathbf{v}_2$ is the relative velocity vector, rotated by the collision through an angle θ; $\mathbf{v}_r = \mathbf{w}_1 - \mathbf{w}_2$, where $\mathbf{w}_1$ and $\mathbf{w}_2$ are velocities of particles 1 and 2 with respect to the center of mass. After the elastic collision these become $\mathbf{w}_1'$ and $\mathbf{w}_2'$ (unchanged in magnitude). The velocity of the scattered particle of type 1 (that is, the type detected) is $\mathbf{v}_1'$, detected at an angle θ_a by the detector in the plane.

Simple considerations of geometry and conservation of momentum lead to various desired relations between quantities in the apparatus and center-of-mass systems, such as (*13–15*)

$$\theta_a = \arctan \left[\frac{\sin\theta + (v_2/v_1)\,(1-\cos\theta)}{(m_1/m_2) + \cos\theta + (v_2/v_1)\sin\theta}\right] \qquad (7)$$

and

$$\theta = \arccos\,[(2w_1^2 - v_1^2 - v_1'^2 + 2v_1\,v_1'\cos\theta_a)/\,2w_1^2] \qquad (8)$$

where

$$w_1 = m_2\,(v_1^2 + v_2^2)^{1/2}/(m_1 + m_2),$$

$$v_1' = v_c\cos(\alpha - \theta_a) \pm [w_1^2 - v_c^2\sin^2(\alpha - \theta_a)]^{1/2},$$

$$v_c = m_1^2\,v_1^2 + m_2^2\,v_2^2)^{1/2}/(m_1 + m_2),$$

and

$$\alpha = \arctan\,(m_2\,v_2/m_1\,v_1).$$

It is found also that

$$\frac{\mathrm{d}\Omega_a}{\mathrm{d}\Omega} = \left(\frac{w_1}{v_1'}\right)^2 \cdot |\cos\zeta| = w_1\,(w_1^2 + v_1'^2 - v_c^2)/2\,v_1'^3 \qquad (9)$$

Of course, in the more general case in which inelastic scattering (including chemical reaction) or out-of-plane detection (or both) is involved, slightly more complicated relations are obtained (*14, 16, 17*).

Thus, a certain amount of manipulation is required in order to convert observed scattered intensities to differential cross sections of theoretical interest. It is to be noted, however, that for systems of mass ratio $m_1/m_2 << 1$, the center-of-mass conversion factors become merely small "corrections" to the observations.

Apparatus

It is not possible to review here the extensive developments in molecular-beam-scattering technology which followed the primitive experiments of Dunoyer. However, it would be a serious omission not to pay homage to the experimental ingenuity of the Hamburg group of the mid-1920's led by O. Stern and F. Knauer, which included J. B. Taylor, I. I. Rabi, B. Lammert, I. Estermann, T. E. Phipps, O. Frisch, and others, who devised the all-important practical techniques of producing, controlling, and detecting beams of neutral particles. Excellent recent reviews dealing, at least in part, with the experimental methods of molecular beam research include those by Ramsey (*18*), Kusch and Hughes (*19*), Pauly (*20*), Trischka (*21*), and Fite and Datz (*22*). Thus this discussion is limited to a brief account of techniques and cursory descriptions of some scattering apparatus in current use.

In general, five classical elements are essential to any molecular-beam-scattering apparatus: (i) high vacuum chamber; (ii) beam source; (iii) collimator; (iv) scattering gas; and (v) detector.

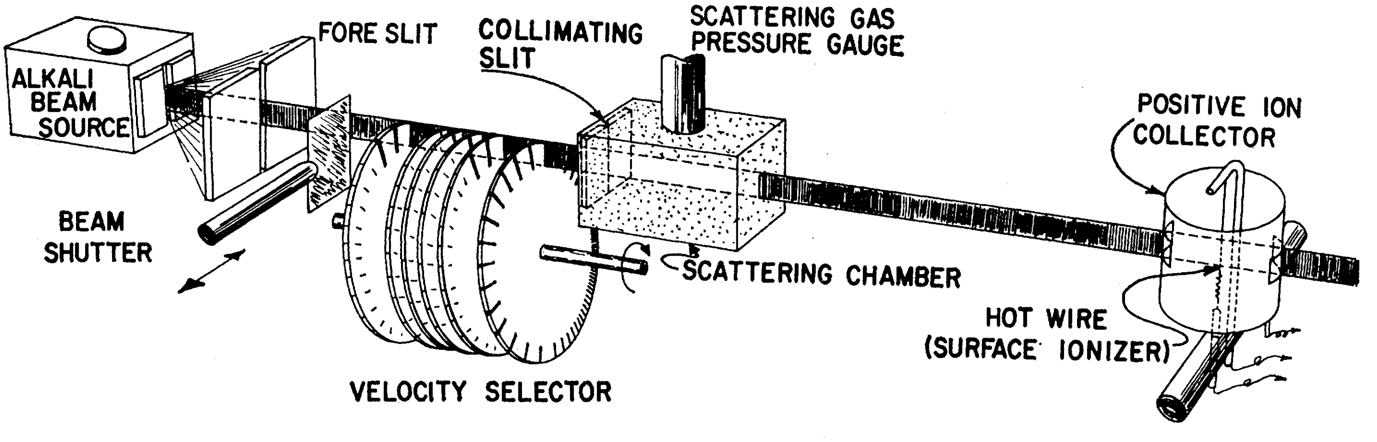

Fig. 2. Diagram of apparatus (*23*) for measuring the velocity dependence of the total cross section for scattering of alkali atomic beams.

Certain additional techniques, more recently introduced, are the following: (vi) crossed-beam arrangement, useful in connection with measurements of angular distributions of scattering; (vii) beam modulation and phase-sensitive detection, to allow discrimination against background; (viii) velocity selection (and analysis), to achieve more nearly monochromatic beams; (ix) rotational-state selection (and analysis), making possible studies of molecules in specified internal quantum states; and (x) selective detection (and mass analysis), permitting observation of chemical reactions.

Let us confine our attention here to scattering apparatus involving velocity-selected beams.

Figure 2 is a pictorial diagram of an apparatus (*23*) for measuring the velocity dependence of the total cross section, $Q(v_r)$. The primary beam (here consisting of easily detectable alkali atoms) effuses into a high vacuum from the oven source slit, is collimated, and then passes through a rotating slotted-disk velocity selector into a chamber containing the scattering gas at a known pressure (about 10^{-4} torr), passing thence to the detector (a Langmuir-Taylor surface ionizer).

Figure 3 shows the arrangement of a crossed-beam apparatus (*24*) for measuring the velocity dependence of the angular distribution of the scattering [that is, the differential cross section $I(\theta)$]. The primary beam (*A*) is velocity-selected (*S*); the secondary beam (*B*) consists usually of a gas of high molecular weight issuing from a low-temperature source (thus, the absolute spread in its velocity distribution will be small, and the consequent effect on the breadth of the distribution of

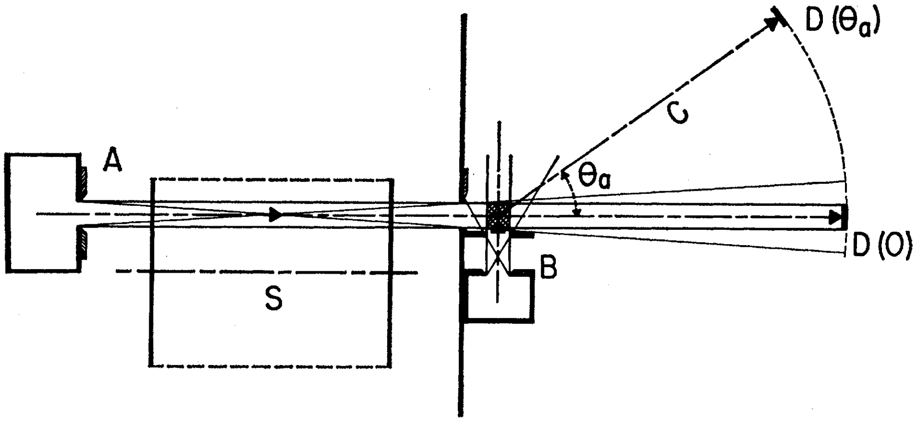

Fig. 3. Arrangement of crossed-beam apparatus (*24*) for measuring the velocity dependence of the angular distribution of scattering.

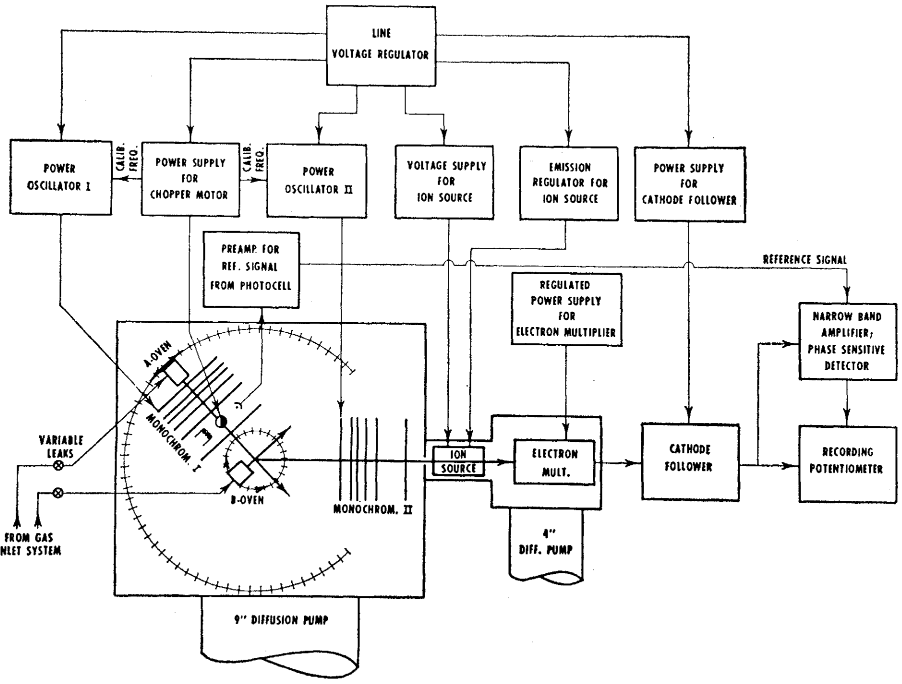

Fig. 4. Schematic diagram of general apparatus (*25*) for measuring differential and total cross sections employing velocity selection and analysis.

relative velocities negligible). The scattered beam (*C*) strikes the detector (*D*) (mounted on a goniometer) located in the plane of the beams at an angle θ_a. The cross-hatched region indicates the overlap of the umbras of the *A* and *B* beams, constituting the major part of the "scattering zone."

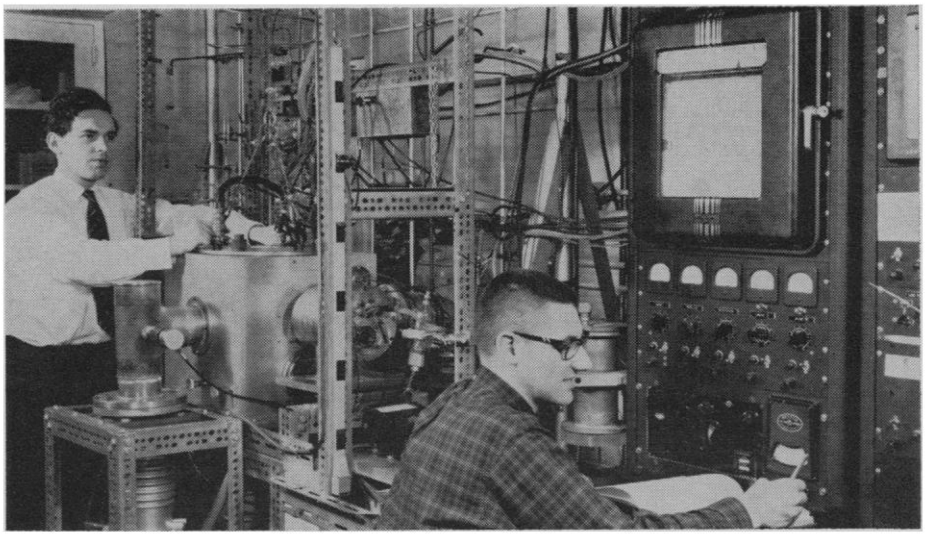

Fig. 5. The apparatus of Fig. 4 in use. Shown are Dr. A. R. Blythe (standing) and Dr. P. J. Groblicki (seated).

Figure 4 is a schematic diagram of a more general apparatus (*25*) for measuring differential and total cross sections for elastic and inelastic scattering. The system employs a velocity selector (monochromator I) and a velocity analyzer (monochromator II) with fixed detector and movable beam system. Either surface-ionization or electron-impact detection may be used; the ion current is amplified by a 12-stage electron multiplier. The primary beam is mechanically modulated at 25 cy/sec; the alternating-current signal is fed to a narrow-band tuned amplifier, thence to the phase-sensitive rectifier and recorder. The detection sensitivity of the apparatus (at a signal-to-noise ratio of 1) is of the order of 100 atoms per second for beams of potassium or cesium. Figure 5 shows the apparatus in use.

Figure 6 is a schematic diagram of the apparatus of Bennewitz, Kramer, Paul, and Toennies (*26*) for measuring the scattering of polar diatomic molecules in selected rotational states (j,m). One quadrupole field is used for the j,m focusing and another for state analysis. The apparatus includes a velocity selector and a mass spectrometer detector.

Scope of Thermal Molecular-Beam-Scattering Studies

We may summarize the various kinds of scattering studies and the information which may be derived from them as follows.

I. Elastic scattering.

a) Atom-atom. Yields information primarily on the long-range attractive potential; with less sensitivity, on the potential well, the number of di-atom bound states, and the steepness of the repulsion.

b) Atom-molecule. Same as *a*; also, gives information on the anisotropy of the long-range potential.

c) Molecule-molecule. Same as *a*; also yields information on the direct dipole-dipole interaction, but the interpretation has not yet been fully developed.

II. Inelastic scattering (energy transfer without chemical reaction).

a) Atom-molecule.

1) Vibrational excitation ($v \rightarrow v'$). Gives information on the short-range repulsive potential.

2) Rotational excitation ($j,m \rightarrow j',m'$). Yields information on the strength and anisotropy of the potential.

b) Molecule-molecule. Same as *a*, but the interpretation has not been fully developed.

III. Reactive scattering.

a) Atom-molecule. Yields information primarily on the energy dependence of the total reaction cross section and on reaction probability versus impact parameter (or distance of closest approach) and collision energy; secondarily, gives restrictions on orientation, product quantum states, and lifetime of complex.

b) Molecule-molecule. Same as *a*, but the interpretation has not yet been fully developed.

Up to the present, most of the experimental work has been in the field of elastic scattering, with a view toward elucidation of the interaction potential. However, there has been ever-increasing activity in the area of reactive scattering (*17, 22, 27–32*) since the pioneering experiments of Taylor and Datz (*27*) on the K + HBr reaction. With the continuing development of sensitive, selective detectors, it should soon become possible to study in depth a variety of basic chemical reactions. One of the most important of these is the atom-molecule reaction of hydrogen, studied by the crossed-beam technique in two laboratories. Datz and Taylor (*31*) reported results on the reaction $D + H_2 \rightarrow DH + H$, while Fite and Brackmann (*32*) investigated the complementary reaction $H + D_2 \rightarrow HD + H$. Although neither the results nor the interpretations offered are yet definitive, it is clear from this example alone that the molecular-beam method is soon to play a crucial role in the future of fundamental chemical kinetics.

In the field of nonreactive inelastic scattering, the first experimental results are those of Toennies (*33*), who observed directly rotational transitions ($j = 3 \rightarrow 2$) in thallium fluoride beams upon collision with a number of atomic and molecular gases. It is of interest to note from these results the rather large rotational-transition cross sections observed for scattering of thallium fluoride by polar molecules. Similar experimental work in the direction of vibrational and rotational excitation is now being carried on in several laboratories (*34*).

Up to this point some of the more general aspects of molecular beam scattering have been treated in a broad way. The remainder of this article is confined to a review of recent developments in the rather more specialized field of elastic scattering at thermal energies (*35, 36*). These may be summarized as follows (in each item the observations are given first, the inferences second, after the colon).

1) From the angular distribution of the scattering at low angles, $I(\theta) \propto \theta^{-7/3}$: the functional form of the long-

range or van der Waals attraction $V = -C/r^6$.

2) From the velocity dependence and magnitude of the total cross section, $Q \propto (C/v)^{2/5}$: the inverse 6th power r-dependence (as in item 1) and the potential constant C.

3) From the cross sections for scattering, by atoms, of polarized beams of atoms or molecules: the angle-dependence or anisotropy of the van der Waals potential.

4) From the rainbow effect in $I(\theta)$ [that is, the maximum in the differential cross section at a characteristic "rainbow angle," $\theta_r = f(\frac{1}{2}\mu v^2/\varepsilon)$]: the depth of the potential well, ε.

5) From de Broglie interference in the angular distribution [that is, undulations in $I(\theta)$]: the equilibrium interparticle separation, r_m.

6) From extrema in $Q(v)$ (deviations from monotonic velocity dependence of the total cross section): the product εr_m, and thus, from absolute values of Q, the value of r_m.

7) From the indexing of maxima in elastic atom-atom impact spectra, (plots of $vQ^{5/2}$ versus $1/v$): a lower limit on the number of vibrational bound states of the di-atom.

Recent Advances in Elastic Scattering at Thermal Energies

The foregoing seven points will now be discussed in greater detail.

1) *Low-angle differential cross sections: evidence for inverse 6th power attraction.*

Classical small-angle deflection theory predicts, for a potential $V = -C/r^s$, a low-angle differential cross section of the form

$$I(\theta) \propto \left(\frac{C}{E}\right)^{2/s} \theta^{-2(1+1/s)} \qquad (10)$$

where $E = \frac{1}{2}\mu v^2$ is the collision energy. Thus, for a long-range inverse 6th power attraction, the low-angle dependence should be $I(\theta) \propto \theta^{-7/3}$. Analysis shows that for typical systems at thermal energies this result should be valid for angles in the range (*37*) from, say, 1 to 10 degrees (center-of-mass system). Experimental results (*38–40*), often presented in the form of log-log plots of $I(\theta)$ (see Fig. 7), have indeed been found to yield low-angle slopes of $-7/3$, in accord with the exponent $s = 6$. Although the accuracy with which such data establish the exponent is only fair, due to considerations of sensitivity (*41*), all experimental results to date support the proposed inverse-6th-power functional form of the van der Waals attraction.

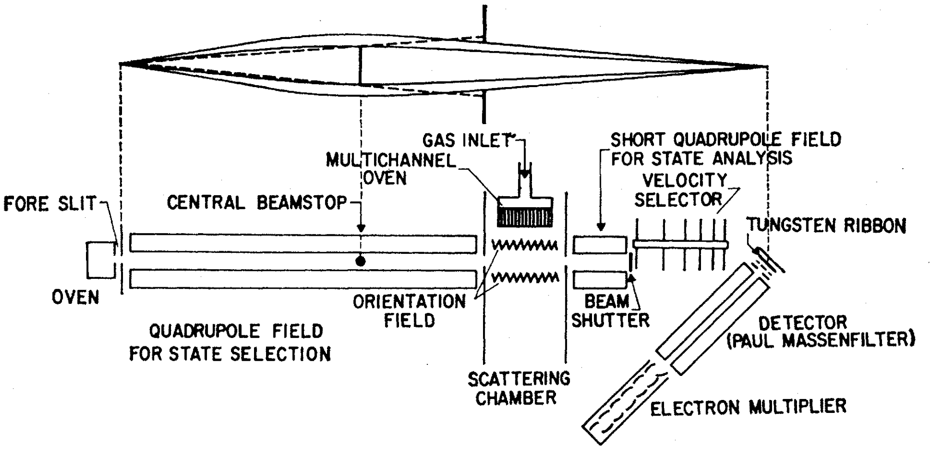

Fig. 6. Schematic diagram of apparatus (*26*) for measuring scattering of molecules in selected rotational states.

2) *Velocity dependence of total cross sections: evidence for inverse 6th power attraction.*

Massey and Mohr (*42*) were the first to develop, on a quantum-mechanical (partial-wave) basis, a reasonable approximation formula for the total cross section for scattering by an inverse sth power potential. Later, using somewhat different approximations, Schiff (*43*) and Landau and Lifshitz (*44*) produced somewhat improved (*45*) approximation formulas for Q. All are of the same form, however—namely,

$$Q = p(s)\left(\frac{C}{\hbar v}\right)^{2/(s-1)} \qquad (11)$$

where v is the relative velocity, $\hbar = h/2\pi$, and $p(s)$ is a numerical factor. For $s = 6$, Eq. 11 becomes

$$Q = 8.08\left(\frac{C}{\hbar v}\right)^{2/5} \qquad (12a)$$

or

$$C = 5.68 \times 10^{-30}\, vQ^{5/2} \qquad (12b)$$

(where v is expressed in cm sec^{-1}, C in erg·cm^6, and Q in cm^2).

The velocity dependence of the cross section predicted by Eqs. 12*a* and 12*b* has been tested experimentally for a number of heavy-particle systems (see *36*). Log-log plots of Q versus v are found to be essentially linear with slopes of $-2/5$. Figure 8 is the first such plot [by Pauly (*7*)] which refers to the scattering of a velocity-selected beam of potassium by nitrogen (*46*).

A problem arises, however, when one considers such experiments for light-particle systems (of low reduced mass μ). There are significant undulatory deviations (*47–51*) from the monotonic $v^{-2/5}$ dependence of Q at lower velocities. These deviations are associated with the existence of a minimum in the potential function. These extrema are of considerable interest and are discussed later.

Another complication arises at higher velocities, where the direct influence of the repulsive part of the potential becomes important (*52*): the velocity dependence of the cross section changes from $v^{-2/5}$ to a nearly flat dependence

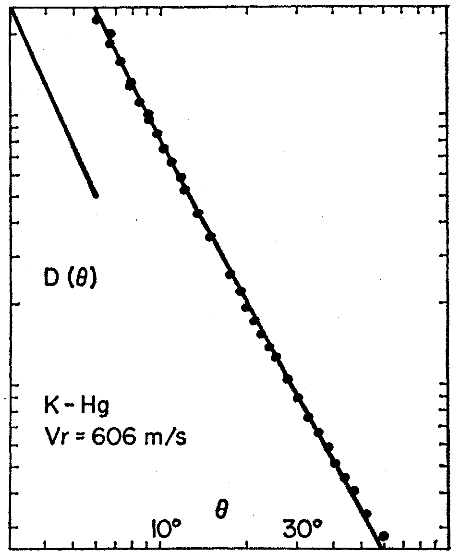

Fig. 7. Log-log plot (*39*) of the angular distribution of the scattering of a velocity-selected potassium beam by a crossed beam of mercury.

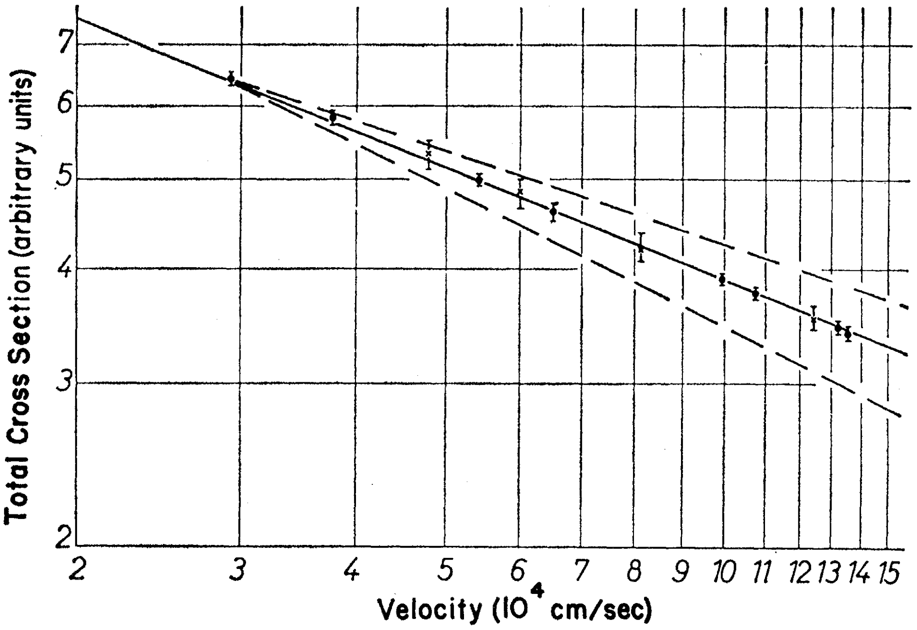

Fig. 8. Log-log plot (*7*) of the velocity dependence of the total cross section for the scattering of potassium by nitrogen. The solid line has a slope of $-2/5$, corresponding to $s = 6$; the dashed lines (shown for comparison) have slopes corresponding to $s = 5$ and $s = 7$, respectively.

(for example, $v^{-2/11}$ for an r^{-12} repulsion) at very high velocities (that is, $v > \varepsilon r_m/\hbar$).

Because of these factors one must be cautious in interpreting cross-section data. A log-log plot of $Q(v)$ should be prepared, showing the range of v over which the slope of the mean curve through the undulations is $-2/5$ (that is, the "low-velocity" region). Over this range the apparent value of C should be plotted against $1/v$ (in such a plot, termed an elastic atom-atom impact spectrum, the extrema are nearly evenly spaced). The true C is then the average value for C_{app} over the low-velocity range. (For experiments at thermal energies with Maxwellian beams, the velocity-averaging has already been effectively accomplished, hence the apparent value of C is close to the correct value.)

It is of interest to compare the "experimental" values for C thus obtained with predictions based on perturbation-theory calculations (*53*). A detailed comparison for alkali-rare gas systems is presented in (*36*). Here it is enough to state that the experimental (*54*) values for C appear consistently larger than the theoretical (*55*) ones. The origin of the discrepancy could well be a systematic, common experimental error (of about 30 percent) in the cross sections; on the other hand, it may be that the attraction is somewhat stronger than that predicted from the perturbation theoretical calculations. Clearly, a definitive, absolute experimental determination of at least one "reference" cross section is needed.

3) *Scattering of polarized beams: anisotropy of the van der Waals potential.*

With the development of high-precision techniques for the measurement of cross-section ratios, the Bonn University group (under the leadership of W. Paul) has succeeded in measuring relative cross sections for the scattering, by atoms, of atoms in selected Zeeman states (*56, 57*) and molecules in specified rotational states (*26, 58*). From these data it has been possible to deduce the anisotropy (angle-dependence) of the van der Waals (r^{-6}) potential for the particular systems investigated.

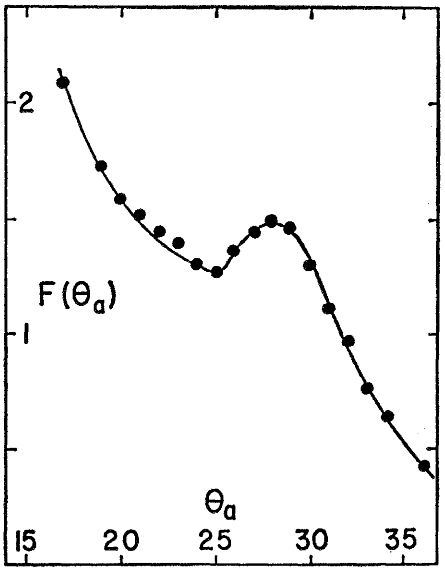

Fig. 9. Plot of observed scattered intensity (*39*) *vs.* lab angle, showing detail of a rainbow maximum. K–Hg system, $v_r = 1.0 \times 10^5$ cm/sec.

The long-range attractive potential between atoms is spherically symmetrical if both atoms are in S-states; however, if one atom is in a state of orbital angular momentum $L \geq 1$, the potential may be anisotropic. For the interaction of an S-state atom with one in a P-state, the van der Waals potential is of the form (see *57*)

$$V_{J,M}(r, \theta) = -\frac{C}{r^6}\left\{ b_{J,M}(\kappa)\,[1 + a_{J,M}(\kappa)\cos^2\theta] \right\} \quad (13)$$

where θ is the angle between the axis of space quantization and the radius vector $\mathbf{r}$; κ is a constant depending only on the electronic structure of the P-state atom; $b_{J,M}(\kappa)$ is a parameter (close to unity) which is dependent on the particular (J, M_J) state of the P-atom; and $a_{J,M}(\kappa)$ is the anisotropy parameter.

The experiments of Berkling, Schlier, and Toschek (*56, 57*) with polarized beams involved the scattering, by various rare gases, of atoms of gallium $4^2P_{3/2}$ (the upper of the ground-state doublet levels) in selected Zeeman states: $|M_J| = 1/2$ and $3/2$. The quantization axis, determined by the magnetic field, was perpendicular to the direction of the gallium beam, yielding so-called "transverse polarization." It was possible to measure the fractional difference between the cross sections $Q_{3/2\ 1/2}$ and $Q_{3/2\ 3/2}$ (where the subscripts refer to J and $|M_J|$, respectively); the results were 1.0, 0.8, and 2.0 percent, respectively, for scattering by xenon, argon, and helium [after suitable processing (*8*) of the data so that the results refer to collisions for which $\mathbf{v}_r$ is perpendicular to the polarization axis]. Schlier's (*57*) theoretical analysis yielded the approximation formula

$$Q_{J,M} = Q \cdot b_{J,M}{}^{2/5}\,(1 + a/6) \qquad (14)$$

where Q is the Schiff-approximated cross section for a spherically symmetrical potential.

Hartree-Fock wave functions were used to calculate the matrix elements necessary for the estimation of κ for gallium, and a difference (ΔQ) of 1.4 percent, independent of the scattering gas, was predicted. This result is in fair

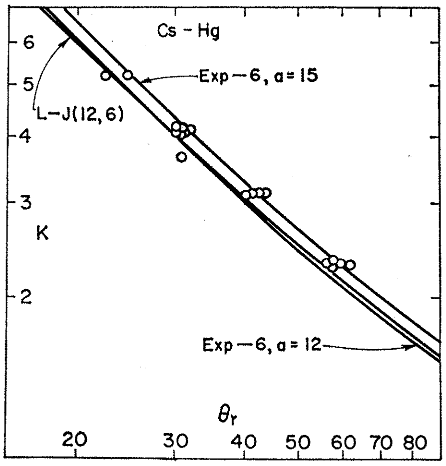

Fig. 10. Energy dependence of the rainbow angle θ_r for the Cs–Hg system (*39*). The curves are calculated for the indicated potentials; the points represent experimental data, assuming $\epsilon = 7.7_2 \times 10^{-14}$ erg.

accord with the observations and lends support to the theoretical treatment.

A somewhat analogous study was carried out by Bennewitz, Kramer, Paul, and Toennies (*26, 58*) on the scattering of polarized molecular beams of thallium fluoride by rare gases. They employed an electric quadrupole field to focus various (j,m_j) rotational states (see Fig. 6). The (j,m_j)-selected molecules—for example, those in the (1,0) state—are allowed to pass through a scattering chamber, consisting of a multichannel oven arranged with the direction of the scattering atomic beam ($\mathbf{v}_A$) perpendicular to the molecular beam. Since it is necessary that the molecules be in a well-defined rotational state relative to the scattering atomic beam, a homogeneous electric field (**E**) is required in the scattering chamber to maintain the molecular orientation axis. This orientation field may be arranged to be either parallel to the direction of the atomic beam (position //) or perpendicular (position ⊥). In the // configuration the molecules are in the (1,0) state, while in the ⊥ arrangement they are in a linear combination of (1,+1) and (1,−1) states with respect to $\mathbf{v}_A$. By measuring the ratio of the cross section $Q_\perp/Q_{||}$ and extrapolating to the proper limit (speed of molecules << speed of atoms—that is, molecules essentially at rest) to yield $Q_{1,1}/Q_{1,0}$, it was possible to deduce the anisotropy parameter q in the van der Waals potential:

$$V(r,\theta) = -\frac{C}{r^6}\left[\frac{1+q\cos^2\theta}{1+\frac{1}{3}q}\right] \qquad (14)$$

Here θ is the angle between the molecular axis and the radius vector **r**, and C is the usual orientation-averaged inverse-6th-power potential constant. According to the theory presented, the cross-section ratio $Q_{1,1}/Q_{1,0}$ depends only on q and should be independent of the particular scattering atom. The observed ratio was 1.014 ± 0.002 for krypton and argon but somewhat smaller for neon and helium. From this value the anisotropy of the thallium fluoride molecule could be deduced; the result was found to be $q = 0.40 \pm 0.07$.

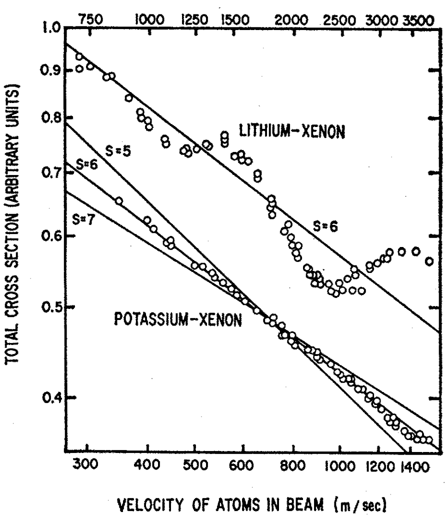

Fig. 12. Log-log plot of $Q(v)$ for scattering of velocity-selected beams of lithium and potassium by xenon (*47*). Note the extrema in the case of Li-Xe. Slopes of the lines for the K–Xe system correspond to $s = 5$, 6, and 7, respectively; for the Li–Xe system, the line drawn is for $s = 6$. The ordinate scales for the two systems are arbitrary and unrelated.

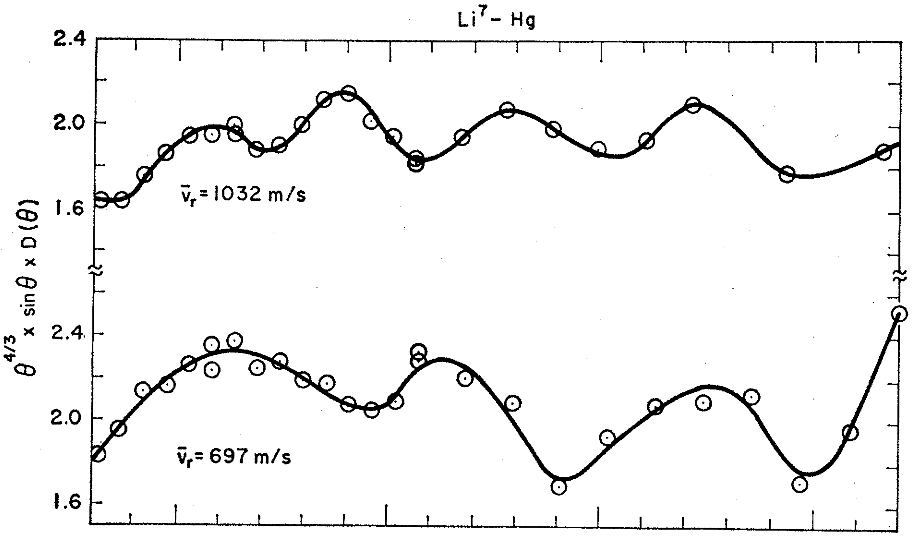

Fig. 11. Undulatory behavior of the angular distribution for the scattering of a velocity-selected beam of lithium by a crossed beam of mercury (*67*); this presentation of the data removes the steep angular dependence, allowing precise location of the extrema angles.

Thus, through the efforts of the Bonn group, the scattering of polarized atomic and molecular beams has become both experimentally feasible and theoretically fruitful; one can expect increased activity in this area in the near future.

4) *Rainbow scattering effect and the potential well depth.*

For any realistic potential with a van der Waals well, the classical angular deflection function $\theta(b,E)$ passes through a minimum at an angle θ_r, designated (*59*) the "rainbow angle." (Here b is the impact parameter and E is the collision energy.) Mason (*60*) first pointed out (by means of a classical analysis) that, as a consequence of the minimum in $\theta(b)$, the angular distribution of the scattering should exhibit a singularity at θ_r, followed by a sharp falloff in intensity at larger angles. Since θ_r is strongly dependent on the ratio $K = E/\varepsilon$, its location could be used to deduce the well depth ε. Ford and Wheeler (*59*) analyzed the phenomenon semiclassically and showed that in the semiclassical limit this singularity becomes a broad maximum shifted to lower angles, with θ_r located near the inflection on the outer side of the maximum.

The rainbow effect has now been observed for a number of systems (*61,*

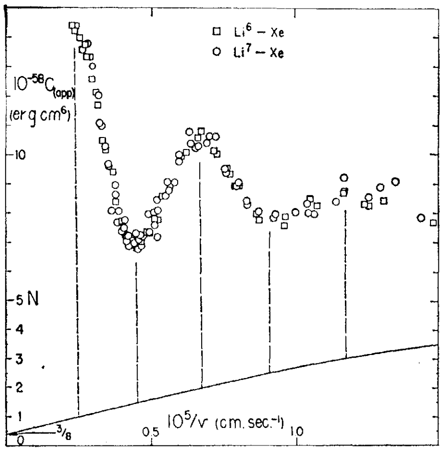

Fig. 13. Plot of an elastic atom-atom impact spectrum for the Li^6–Xe and Li^7–Xe systems, from the data of Rol and Rothe (*48*).

62). Figure 9 shows a well-resolved rainbow maximum for the K–Hg system. Figure 10 shows the energy dependence of θ_r for the Cs–Hg system, as compared with the theoretical behavior (*63, 64*).

In Table 1 are listed values of ε obtained by the rainbow scattering method, together with two confirmatory values determined in other ways.

Since the rainbow scattering effect is a semiclassical phenomenon it should be applicable to many heavy-particle systems as a method for determining van der Waals well depths.

5) *De Broglie interference (undulations) in the angular distribution, and the estimation of* r_m.

When the de Broglie wavelength $\lambda = h/\mu v$ of the colliding system is of the same order of magnitude as the "range" of the interatomic forces, oscillatory interference effects in the angular distribution of the scattering are to be expected (*65–67*). Observations of such interferences in atomic beam scattering had not been reported until recently (*68*), however, because of rigorous experimental requirements, such as beam monochromaticity and angular resolution. Figure 11 shows some recent data (*67*) (for velocity-selected beams of lithium scattered by crossed beams of mercury), plotted with an ordinate which is essentially $\theta^{7/3} \cdot I(\theta)$. (This presentation removes the steep angular dependence of the angular distribution and allows precise estimation of the angles of the interference maxima and minima.)

Theoretical calculations by the wave mechanical method (*65, 66*) have yielded $I(\theta)$ as a function of a velocity parameter A (which is proportional to the ratio r_m/λ) for various assumed Lennard-Jones potential constants, to compare with the experimental undulation pattern. As discussed elsewhere (*66*), in the case of two isotopic systems (1 and 2), the same diffraction pattern should be obtained if $\lambda_1 = \lambda_2$. Experiments (*67*) in which the behavior of Li^6 was compared with that of Li^7 have confirmed this expectation.

Since the pattern of the angular distribution is governed primarily by the parameter A and only secondarily by the depth of the potential well, it is possible to estimate r_m by comparing the periodicity of calculated curves for $I(\theta)$ plotted against A with observed angular distributions at specified de Broglie wavelengths.

Table 1. Potential well depths. (Reference numbers in parentheses.)

System	10^{14} ε (erg)	
	Rainbow method	Other
Cs–Hg	7.7* (*14*)	
K–Hg	7.5* (*14*)	8.3* (*74*)
K–Kr	1.2_5† (*15*)	1.3* (*69*)
K–HBr	3.8_5† (*17*)	
K–CH$_3$Br	2.3_5† (*29*)	

* Assumed potential, Lennard-Jones (12,6).
† Assumed potential, Exp (12,6).

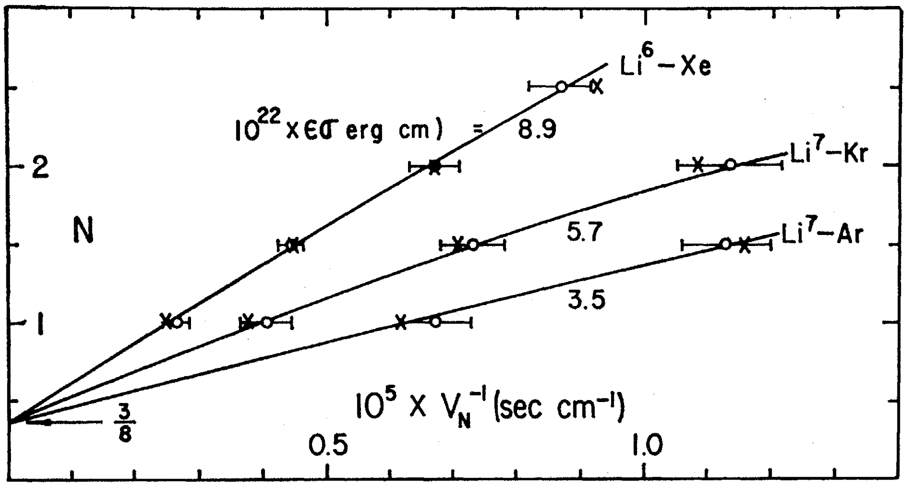

Fig. 14. Summary of plots of extrema for the Li–Xe, Li–Kr, and Li–Ar systems (*51*); N is plotted against $1/v_N$. The brackets indicate the limits of experimental uncertainty. The values of $\varepsilon\sigma$ shown are those obtained from the limiting slopes ($1/v_N \rightarrow 0$). The crosses indicate the values predicted from the full theoretical analysis, on the basis of an assumed Lennard-Jones (12,6) potential with $\varepsilon\sigma$ = 9.47, 6.09, and 3.82 (10^{-22} erg cm) for the Li-Xe, Li-Kr, and Li-Ar systems, respectively.

Once it becomes possible to resolve the oscillations in the angular distribution for a given system, the process of "converging" on the correct potential $V(r)$ is considerably facilitated—that is, the potential is, in principle, overdetermined by the large number of information bits extracted from the pattern (locations) of the interferences in $I(\theta)$ over a range of velocities. The procedures described should be especially useful in elucidating the potential for systems of low reduced mass and weak van der Waals attraction.

6) *Extrema in* Q(v) *and the evaluation of the product* εr_m.

Undulatory deviations from the monotonic $v^{-2/5}$ dependence of the total cross section, mentioned in section 2, were predicted (*49, 66*), and have now been observed, for the systems Li–Hg (*67*), Li–Xe (*47, 48*), Li–Kr and Li–Ar (*48*), and K–Kr (*69*). Figure 12 is a graph from the experiments of Rothe *et al.* (*47*). Figure 13 is a plot of an elastic atom-atom impact spectrum, as described in section 2, constructed from the data of Rol and Rothe (*48*), for Li^6–Xe and Li^7–Xe.

In Fig. 13 the extrema are indexed starting with the first high-velocity maximum for which $N = 1$, and so on. Their locations are correlated by the lower curve (N plotted against $1/v$). According to the theory (*50*), such a plot should be nearly linear, with a high-velocity intercept of 3/8 and a limiting slope proportional to the product εr_m. Figure 14 gives a summary of such extrema plots for the Li–Xe, Li–Kr, and Li–Ar systems (*51*). In analyzing the data, a Lennard-Jones (12,6) potential was assumed; the values that adjoin the curves refer to the product $\varepsilon\sigma$, where σ is the first zero of the potential ($\sigma = r_m/2^{1/6}$).

As more data and better methods of analysis become available it appears that it will be possible to go beyond the simple two-parameter Lennard-Jones

(12,6) potential. Mueller (*70*) has concluded, on the basis of a reanalysis of Knauer's (*12*) I(θ) data on the H_2–Hg system, that the minimum in the potential should be broader than the Lennard-Jones well. Pauly (*71*) has reanalyzed the $Q(v)$ data for the Li–Kr system (*48, 51*) in terms of a three-parameter Kihara potential and has achieved a better fit of the calculated to the observed extrema amplitudes.

Quite analogous to the discussion presented in section 5, observations of multiple extrema in atom-atom impact spectra will assist in achieving a desirable "overdetermination" of the van der Waals potential (*72*).

7) *Maxima in atom-atom impact spectra and number of vibrational states of the di-atom.*

Analysis (*49, 50*) of the extrema in elastic atom-atom impact spectra has indicated that the maxima serve as "counters" of the vibrational states of the di-atom. A bound-state rule has been proposed (*50*), as follows. The observation of m maxima in the elastic atom-atom impact spectrum implies the existence of at least m vibrational states for the di-atom.

It has also been shown (*50*) that there is a one-to-one correspondence between the particular extremum index N and the vibrational quantum number v: thus, $N - 1 \longleftrightarrow v$.

It is important to recognize that this "level counting" technique is not dependent on the detailed form of the potential assumed, and that it should therefore have considerable generality. [Its usefulness will, of course, be limited by the experimental difficulty of resolving the maxima and by the possible loss of detail when inelastic and elastic processes (*73*) are concurrent.] It is also of interest to note that from the atom-atom impact spectra we can learn about the bound states of di-atoms which may be so very weakly associated (so unstable) as to be unavailable for study by any of the conventional molecular spectroscopic methods.

Concluding Remarks

Studies of thermal molecular-beam scattering fall into three categories: elastic, inelastic, and reactive scattering. Most of the research up to the present has dealt with elastic scattering, which has therefore received the greatest attention in this article. By virtue of their very complexity, however, the fields of inelastic and reactive scattering hold much promise and excitement; important advances in these areas will surely be forthcoming at an increasing rate in the near future. Nevertheless, it is clear that underlying these developments must be a fundamental understanding of intermolecular forces, obtained at least in part through studies of elastic scattering of atomic and molecular beams.

Reference and Notes

1. L. Dunoyer, *Compt. Rend.* **152**, 592 (1911); *Radium, Paris* **8**, 142 (1911); *Compt. Rend.* **157**, 1068 (1913); *Radium, Paris* **10**, 400 (1913).
2. M. Born, *Physik. Z.* **21**, 578 (1920); F. Bielz, *Z. Physik.* **32**, 81 (1925); F. Knauer and O. Stern, *ibid.* **39**, 764, 780 (1926); ———, *ibid.* **53**, 766 (1929).
3. A. Ellett and R. M. Zabel, *Phys. Rev.* **37**, 1112 (1931); W. H. Mais and I. I. Rabi, *ibid.* **43**, 378 (1933); R. G. J. Fraser and L. F. Broadway, *Proc. Roy. Soc. London, Ser. A* **141**, 626 (1933); L. F. Broadway, *ibid.*, p. 634; W. H. Mais, *Phys. Rev.* **45**, 773 (1934); N. Sasaki, E. Nishibori, H. Uchida, *J. Chem. Soc. Japan* **57**, 1277 (1936); N. Sasaki, E. Nishibori, G. Kondo, K. Kodera, *ibid.*, p. 1284; P. Rosenberg, *Phys. Rev.* **55**, 1267 (1939); ———, *ibid.* **57**, 561 (1940).
4. S. Rosin and I. I. Rabi, *Phys. Rev.* **48**, 373 (1935).
5. I. Amdur and H. Pearlman *J. Chem. Phys.* **8**, 7 (1940) (the first of an extensive series by Amdur and his colleagues on high-energy molecular beam scattering).
6. For typical atoms and molecules in the thermal energy region (< 1 ev), values of Q may lie in the range 1000 $Å^2$ to 10 $Å^2$, while at higher energies (up to the kilovolt region) Q decreases slowly, tending toward values of the order of 1 $Å^2$.
7. H. Pauly, *Z. Naturforsch.* **15a**, 277 (1960).
8. K. Berkling, R. Helbing, K. Kramer, H. Pauly, C. Schlier, P. Toschek, *Z. Physik* **166**, 406 (1962).
9. It is well known [see, for example, J. O. Hirschfelder, C. F. Curtiss, R. B. Bird, *Molecular Theory of Gases and Liquids* (Wiley, New York, 1954)] that the trajectory of a collision depends sensitively on the impact parameter b (the perpendicular distance between the paths of the two particles at large separation). The most likely collisions are those for which b is large; for these collisions the angular deflection is very small. This gives rise to a predominance of "forward" scattering.
10. F. Knauer, *Z. Phys.* **80**, 80 (1933); ———, *Naturwissenschaften* **21**, 366 (1933); R. M. Zabel, *Phys. Rev.* **46**, 411 (1934).
11. R. M. Zabel, *ibid.* **44**, 53 (1933).
12. F. Knauer, *Z. Phys.* **90**, 559 (1934).
13. R. Helbing and H. Pauly, thesis (Helbing), University of Bonn (1961) (*Z. Physik*, in press).
14. F. A. Morse and R. B. Bernstein, *J. Chem. Phys.* **37**, 2019 (1962).
15. D. Beck, *ibid.*, p. 2884.
16. S. Datz, D. R. Herschbach, E. H. Taylor, *ibid.* **35**, 1549 (1961).
17. D. Beck, E. F. Greene, J. Ross, *ibid.* **37**, 2895 (1962).
18. N. F. Ramsey, *Molecular Beams* (Clarendon, Oxford, 1956).
19. P. Kusch and V. W. Hughes, in *Handbuch der Physik*, S. Flügge, Ed. (Springer, Berlin, 1959), vol. 37, p. 1.
20. H. Pauly, *Fortschr. Physik* **9**, 613 (1961).
21. J. W. Trischka, *Methods Exptl. Phys.* **3**, 589 (1962).
22. W. L. Fite and S. Datz, *Ann. Rev. Phys. Chem.* **14**, 61 (1963).
23. A composite of the designs used by H. Pauly [*Z. Naturforsch.* **15a**, 277 (1960)] and E. W. Rothe, P. K. Rol, S. M. Trujillo, R. H. Neynaber [*Phys. Rev.* **128**, 659 (1962)].
24. A composite of the designs used by H. U. Hostettler and R. B. Bernstein [*Phys. Rev. Letters* **5**, 318 (1960)] and E. F. Greene, R. W. Roberts, J. Ross [*J. Chem. Phys.* **32**, 940 (1960)]. See also F. A. Morse and R. B. Bernstein, *ibid.* **37**, 2019 (1962), and D. Beck, *ibid.*, p. 2884.
25. H. U. Hostettler and R. B. Bernstein, Proceedings of Atomic and Molecular Beams Conference, Denver, 1960; *Rev. Sci. Instr.* **31**, 872 (1960). The assistance of H. F. Schulte with the electronic instrumentation is acknowledged.
26. H. G. Bennewitz, K. H. Kramer, W. Paul, J. P. Toennies, *Z. Physik* **177**, 84 (1964).
27. E. H. Taylor and S. Datz, *J. Chem. Phys.* **23**, 1711 (1955).
28. D. R. Herschbach, G. H. Kwei, J. A. Norris, *ibid.* **34**, 1842 (1961); D. R. Herschbach, *Discussions Faraday Soc.* **33**, 149 (1962).
29. M. Ackerman, E. F. Greene, A. L. Moursund, J. Ross, in *Ninth International Symposium on Combustion* (Academic Press, New York, 1963), p. 669.
30. E. Gersing, E. Hundhausen, H. Pauly, *Z. Physik* **171**, 349 (1963).
31. S. Datz and E. H. Taylor, *J. Chem. Phys.* **39**, 1896 (1963).
32. W. L. Fite and R. T. Brackmann, "Proceedings 3rd International Conference on Physics of Electronic and Atomic Collisions, London, 1963" (North Holland, Amsterdam, in press).
33. J. P. Toennies, *ibid.*
34. Drs. A. R. Blythe, A. E. Grosser, and K. H. Kramer are collaborating with me in this work.
35. The field of elastic scattering has been reviewed through 1961 by Pauly (see *20*); for a detailed summary of recent developments at thermal energies, see *36*.
36. R. B. Bernstein, "Proceedings 3rd International Conference on Physics of Electronic and Atomic Collisions, London, 1963" (North-Holland, Amsterdam, in press).
37. The lower limit on the range is imposed by the well-known failure of the classical treatment at very small angles, leading to an unphysical singularity at $\theta = 0$ and thus to an infinite total cross section. A proper quantum-mechanical approach yields a finite $I(0)$, and Q. Helbing and Pauly (see *13*) investigated with high resolution the very-low-angle scattering behavior for a number of systems, verifying the expected transition from the classical to quantum angular dependence at sufficiently low angles (that is, for $\theta < \lambda/\pi r_0$, where $\lambda = h/\mu v$ is the de Broglie wavelength).
38. See R. Helbing and H. Pauly (*13*) for results for the K–Xe, K–Ar, K–Br_2, and K–CBr_4 systems and others.
39. See F. A. Morse and R. B. Bernstein, *J. Chem. Phys.* **37**, 2019 (1962), for results for the K–Hg and Cs–Hg systems.
40. P. J. Groblicki and R. B. Bernstein, unpublished results for the Li–Hg system.
41. A small uncertainty of, say, ± 1 percent in slope leads to an uncertainty of $\sim \pm 0.4$ in s (near $s = 6$).
42. H. S. W. Massey and C. B. O. Mohr, *Proc. Roy. Soc. London, Ser. A* **144**, 188 (1934).
43. L. I. Schiff, *Phys. Rev.* **103**, 443 (1956).
44. L. D. Landau and E M. Lifshitz, *Quantum Mechanics* (Pergamon, London, 1959), p. 416.
45. For discussion, see R. B. Bernstein and K. H. Kramer, *J. Chem. Phys.* **38**, 2507 (1963).
46. An easily obtainable accuracy of, say, ± 4 percent in the slope of such graphs corresponds to an uncertainty of less than ± 0.2 in s (near $s = 6$), so this procedure is more sensitive than that described in section 1 in establishing the exponent $s = 6$ for the van der Waals attraction.
47. E. W. Rothe, P. K. Rol, S. M. Trujillo, R. H. Neynaber, *Phys. Rev.* **128**, 659 (1962).
48. P. K. Rol and E. W. Rothe, *Phys. Rev. Letters* **9**, 494 (1962).
49. R. B. Bernstein, *J. Chem. Phys.* **37**, 1880 (1962).
50. ———, *ibid.* **38**, 2599 (1963).
51. E. W. Rothe, P. K. Rol, R. B. Bernstein, *Phys. Rev.* **130**, 2333 (1963).
52. R. B. Bernstein, *J. Chem. Phys.* **38**, 515 (1963).
53. Typical values (see *36*) of C (in units of 10^{-58} erg·cm^6) for systems involving potassium beams are as follows (listed in each case are the target gas, the average experimental value for C, and, in parentheses, the theoretical estimate): Ne, 0.69 (0.65); Ar, 5.0 (2.7); Kr, 10.5 (4.0); Xe, 12. (6.5).
54. The experimental data are from the following sources. E. W. Rothe, P. K. Rol, and R. B. Bernstein, (see *51*); R. Helbing and H. Pauly, [*13* and private communication (June 1963)]; E. W. Rothe, L. L. Marino, R. H. Neynaber, P. K. Rol, S. M. Trujillo, *Phys. Rev.* **126**, 598 (1962); D. Beck (see *15*); R.

Schoonmaker, *J. Phys. Chem.* **65**, 892 (1961); E. W. Rothe and R. B. Bernstein, *J. Chem. Phys.* **31**, 1619 (1959); H. Pauly, *Z. Angew. Phys.* **9**, 600 (1957).
55. A. Dalgarno and A. E. Kingston, *Proc. Phys. Soc. London* **73**, 455 (1959); *ibid.* **75**, 607 (1961).
56. K. Berkling, C. Schlier, P. Toschek, *Z. Naturforsch.* **15a**, 838 (1960).
57. ———, *Z. Physik* **168**, 81 (1962).
58. K. H. Kramer, thesis, University of Bonn (1962).
59. K. W. Ford and J. A. Wheeler, *Ann. Phys. N.Y.* **7**, 259 (1959).
60. E. A. Mason, *J. Chem. Phys.* **26**, 667 (1957).
61. See F. A. Morse, R. B. Bernstein, H. U. Hostettler [*ibid.* **36**, 1947 (1962)] and F. A. Morse and R. B. Bernstein (*14*) for results for the K–Hg and Cs–Hg systems; see M. Ackerman, E. F. Greene, A. L. Moursund, and J. Ross (*29*) for results for the K-CH_3Br system.
62. See D. Beck (*15*) for results for the K–Kr and K–HBr systems.
63. Theoretical calculations of $\theta_r(K)$ have been published for the Exp (α,6) potential (*60*) and the Lennard-Jones (12,6) (*14, 62*), the Morse (*36*), and the Kihara potential [the latter by C. Schlier, *Z. Physik* **173**, 352 (1963)].
64. Because of the spread of the theoretical curves associated with different assumed functional forms for the repulsive part of the potential, an accuracy of better than ± 5 percent in ε is unlikely.
65. H. S. W. Massey and C. B. O. Mohr, *Proc. Roy. Soc. London, Ser. A* **141**, 434 (1933); ———, *ibid.* **144**, 188 (1934); R. B. Bernstein, *J. Chem. Phys.* **33**, 795 (1960).
66. R. B. Bernstein, *J. Chem. Phys.* **34**, 361 (1961).
67. P. J. Groblicki and R. B. Bernstein, unpublished results.
68. See H. U. Hostettler and R. B. Bernstein [*Phys. Rev. Letters* **5**, 318 (1960)] for results on the Li–Hg system. Much earlier, Zabel (*11*) had reported angular distributions for a (Maxwellian) helium beam scattered by helium (similarly for H_2) in which the curves evidence a suggestion of a maximum; however, the results are inconclusive.
69. See E. W. Rothe, R. H. Neynaber, B. W. Scott, S. M. Trujillo, P. K. Rol [*J. Chem. Phys.* **39**, 493 (1963)] for analysis of $Q(v)$ for the K–Kr system—that is, from the elastic atom-atom impact spectrum.
70. C. R. Mueller and R. P. Marchi, *J. Chem. Phys.* **38**, 745 (1963); see also, J. W. Brackett, C. R. Mueller, W. A. Sanders, *ibid.* **39**, 2564 (1963) and W. A. Sanders and C. R. Mueller, *ibid.*, p. 2572.
71. R. Düren and H. Pauly, *Z. Physik* **175**, 227 (1963); *ibid.* **177**, 146 (1964).
72. Of course, to obtain reliable information on the repulsive part of the potential one must leave the thermal velocity range and measure cross sections at high energies (>> 1 ev), in accordance with the well-known procedures of Amdur: for example, see I. Amdur and R. R. Bertrand, *J. Chem. Phys.* **36**, 1078 (1962); I. Amdur, J. E. Jordan, S. O. Colgate, *ibid.* **34**, 1525 (1961); I. Amdur, *Planetary and Space Sci.* **3**, 228 (1961); papers in the series referred to in *5*.
73. See, for example, R. B. Bernstein, A. Dalgarno, H. S. W. Massey, I. C. Pervival, *Proc. Roy. Soc. London, Ser. A* **274**, 427 (1963).
74. See E. Gersing, E. Hundhausen, H. Pauly (*30*) for an analysis of the differential scattering of the K–Hg system with Maxwellian beams.
75. Financial support by the U.S. Atomic Energy Commission (Chemistry Branch, Division of Research) is gratefully acknowledged.

Photochromic Silicate Glasses Sensitized by Silver Halides

Their characteristic of changing color reversibly, in combination with other properties, suggests many uses.

W. H. Armistead and S. D. Stookey

The phenomenon of photochromism—change of color on exposure to light—has been studied by many observers. The proceedings of a symposium on this subject were published in the December 1962 issue of the *Journal of Physical Chemistry* (*1*), and Brown and Shaw, in a recent review (*2*), list hundreds of photochromic organic and inorganic substances. There are many potential uses for photochromic substances, provided the special requirements for these uses can be met. True reversibility of the color change—that is, freedom from fatigue with repeated light-and-dark cycling—is a basic requirement for most of these uses. Very few photochromic substances fulfill this requirement.

The action of ultraviolet light or other high-energy radiation is known to cause color changes in many glasses. In most cases the changes are very slow and are irreversible at room temperature. Recently A. Cohen and H. Smith (*3*) reported photochromic silicate glasses, sensitized by the addition of cerium and europium, which showed rapid darkening and fading. These glasses, however, were reported to fatigue with repeated cycling.

In this article we describe a new type of photochromic material that changes color reversibly and has combinations of properties which make it suitable for a number of practical applications. The photochromic materials of this investigation are silicate glasses containing dispersed crystals of colloidal silver halide, precipitated within the homogeneous melt during cooling or reheating.

In the absence of light, the silver halide glass may be either transparent and essentially colorless or opaque white, depending on the particle size and the concentration of the suspended colloid.

Photochromic behavior has been observed in transparent glasses containing silver halide microcrystals as small as 40 angstroms in diameter, and with concentrations of crystals as low as 500 parts per million by volume, as determined by electron microscopy and by small-angle x-ray scattering.

Chemical Composition

Table 1 gives results of chemical analyses of some photochromic silver halide glasses.

The base glasses are generally alkali metal borosilicates; they are sensitized by silver halide microcrystals precipitated from solution in the glass. The total concentration of silver ranges from 0.2 to 0.7 percent (by weight) in the transparent glasses, and from 0.8 to 1.5 percent in opaque glasses. The concentration of the halogen, consisting of chlorine, bromine, and iodine individually or together, ranges upward from a concentration sufficient to react stoichiometrically with a 0.2-percent concentration of silver to form the halide, or halides, to a total concentration of about 0.4 percent in the transparent glasses, and higher in opaque glasses.

The halogen content of these glasses is expressed in terms of the amount

The authors are affiliated with the Corning Glass Works, Corning, N.Y.